Monthly Notices
of the
ROYAL ASTRONOMICAL SOCIETY

MNRAS **486,** 3259–3265 (2019) doi:10.1093/mnras/stz1095

Laboratory formation and photo-chemistry of ionic HBC/anthracene clusters in the gas phase

Junfeng Zhen,[1,2]★ Weiwei Zhang,[3] Yuanyuan Yang[1,2] and Qingfeng Zhu[1,2]

[1]*CAS Key Laboratory for Research in Galaxies and Cosmology, Department of Astronomy, University of Science and Technology of China, Hefei 230026, China*
[2]*School of Astronomy and Space Science, University of Science and Technology of China, Hefei 230026, China*
[3]*Department of Mechanical and Nuclear Engineering, Pennsylvania State University, University Park, PA 16802, USA*

Accepted 2019 April 15. Received 2019 April 12; in original form 2019 February 4

ABSTRACT

In this paper, we present a study of the formation and photo-chemistry of hexa-peri-hexabenzocoronene (HBC, $C_{42}H_{18}$)/anthracene ($C_{14}H_{10}$) cluster cations in the gas phase using experimental and theoretical calculations, and we offer an approach of the evolution of carbonaceous dust grains in the interstellar medium. The experiments, which combined a quadrupole ion trap and time-of-flight mass spectrometry, show that the large cluster cations can form by gas-phase condensation through molecular-ion reactions; that is, from $C_{14}H_{10}DHBC^+$ (e.g. $C_{14}H_{10}C_{42}H_{17}^+$, $m/z = 699$), to $(C_{14}H_{10})_2DHBC^+$ [e.g. $(C_{14}H_{10})_2C_{42}H_{16}^+$, $m/z = 876$] and then to $(C_{14}H_{10})_3DHBC^+$ [e.g. $(C_{14}H_{10})_3C_{42}H_{15}^+$, $m/z = 1053$]. Furthermore, with laser irradiation, the HBC/anthracene cluster cations involve a dehydrogenation process or the loss of its mono-anthracene groups. Based on the results of experiments and quantum chemistry calculations, we demonstrate that large molecular clusters (∼100 atoms, covalently bonded) might be formed via a bottom-up process in the gas phase, and we show that there is a benefit to understanding their photo-chemical behaviour. In addition, the studies of HBC/anthracene clusters (ranging from 83 to 129 atoms or ∼2 nm in size) also provide a way of interpreting nanometre-sized grains in space.

Key words: astrochemistry – molecular processes – methods: laboratory: molecular – ISM: molecules – ultraviolet: ISM.

1 INTRODUCTION

The mid-infrared spectra, observed in the interstellar medium (ISM) with broad features at 3.3, 6.2, 7.7, 8.6 and 11.2 μm, is often recognized as the ultraviolet (UV) pumped fluorescence of polycyclic aromatic hydrocarbon (PAH) molecules (Sellgren 1984; Puget & Leger 1989; Allamandola, Tielens & Barker 1989). Many lines of evidence have shown that PAH clusters are very small dust grains in the ISM (van Diedenhoven et al. 2004; Rapacioli, Joblin & Boissel 2005; Berné et al. 2007). Large PAH clusters or related complex species are believed to be formed by the self-assembly between free gas-phase PAHs and amorphous carbon particles. The evolution of the infrared (IR) spectrum suggests that the UV irradiation generally induces the destruction of fragile aliphatic bonds and the formation of a more aromatic system, which have been commonly thought of as an important role of the interstellar PAH model (Henning & Salama 1998; Rapacioli et al. 2006; Rhee et al. 2007; Tielens 2008).

Various studies on the photo-fragmentation of PAH molecules have been performed in the past decade (e.g. Ekern et al. 1998; Zhen et al. 2014; Castellanos et al. 2018; West et al. 2018). Particularly, the photo-fragmentation behaviour of small PAH cluster cations (∼50 atoms, e.g. pyrene cluster or fluorene cluster) has been reported recently (Zhen, Chen & Tielens 2018; Zhang et al. 2019). Compared with small PAH clusters, the formation process and photo-fragmentation behaviour of large PAH cluster cations ($\gtrsim$100 atoms) are also very important in astrophysical applications, because they are initial forms of carbonaceous dust grains in the ISM (Jäger et al. 2009, 2011). However, there is still a lack of experimental evidence for these processes so far.

Carbonaceous grains are the most abundant cosmic dust components in space, and a major fraction of nanometre-sized carbonaceous grains are formed by means of gas-phase condensation (Henning & Salama 1998). Such carbon particles are usually a blend of different carbon phases, including graphitic, diamond-like, fullerene-like and chain-like components on a sub-nanometre or nanometre scale (Kroto et al. 1985; Becker et al. 1994; van Diedenhoven et al. 2004; Jäger et al. 2011). In the dust model, large PAH clusters might play an important role in the formation pathways

★ E-mail: jfzhen@ustc.edu.cn

© 2019 The Author(s)
Published by Oxford University Press on behalf of the Royal Astronomical Society

Downloaded from https://academic.oup.com/mnras/article-abstract/486/3/3259/5480882 by University of Science and Technology of China user on 05 May 2019

of carbonaceous grains in space from molecular components or clusters (Henning & Salama 1998; Tielens 2008). Chen & Dobbins (2000) have proposed that large PAHs and PAH clusters with a layer structure might be nucleation seeds.

In the PAH-dominated soot formation processes, at high temperatures, the driving force of the cluster growth is the generation of PAH radicals, which are formed by the release of hydrogen atoms from PAHs (Violi & Izvekov 2007; Wang 2011; Elvati & Violi 2013). Then, the dominant pathway of the soot nuclei process is the reaction between PAH radicals and PAHs (Le Page, Snow & Bierbaum 2001; Richter & Howard 2000; Richter et al. 2004). In this paper, we present a study of the formation process of large covalently bonded PAH cluster cations (∼100 atoms), such as the hexa-peri-hexabenzocoronene (HBC, $C_{42}H_{18}$)/anthracene ($C_{14}H_{10}$) cluster, and their photo-fragmentation behaviour. Both experimental and theoretical studies are carried out to improve our understanding of the inherent stabilities of large covalently bonded PAH clusters. We explore HBC/anthracene clusters using experiments with a newly constructed set-up – a quadrupole mass filter (QMF)/quadrupole ion trap source (QIT), analysed by time-of-flight (TOF) mass spectrometry and supported by density functional theory (DFT) calculations. We select anthracene ($C_{14}H_{10}$, $m/z = 178$) for this study, given its potential astrophysical interest (Tielens 2005) and the presence of armchair and zigzag edges that might facilitate the formation of new molecule clusters. HBC ($C_{42}H_{18}$, $m/z = 522$) is an all-benzenoid PAH with a size in the astrophysically relevant range (Tielens 2008; Croiset et al. 2016) that possibly serves as a prototypical example for large(r) PAHs. In addition, the photo-fragmentation behaviour and the IR spectra of HBC^+ and HBC^{2+} have been obtained by Zhen et al. (2014, 2017).

2 EXPERIMENTAL METHODS

We construct a new set-up to perform our experiment, a QMF–QIT–TOF mass spectrometer. In detail, the experimental apparatus consists of three differentially pumped chambers. The first chamber is an ion source chamber (ionso chamber), which includes an oven (Heat Wave Labs) and an electron gun−ion gate system (EGUN, Jordan C-950). The second chamber is an ion trap chamber (iontr chamber) that contains a QIT (Jordan C-1251). The ionso and iontr chambers are connected by a QMF (Ardara), which consists of four 9-mm round rods, preceded by 1-inch pre-filter electrodes, and is fed by a radio-frequency (rf) power supply capable of an m/z in the range of up to 2000. The third chamber is detection equipment, which is a reflection TOF mass spectrometer (Jordan D-850). A 2-mm skimmer is placed between the iontr and TOF chambers. The base pressures in the ionso, iontr and TOF chambers are $\sim 3.0 \times 10^{-8}$, $\sim 3.0 \times 10^{-8}$ and $\sim 4.0 \times 10^{-9}$ mbar, respectively.

HBC is evaporated by heating the powder (Kentax, with a purity better than 99.5 per cent) to the temperature of ∼573 K in the oven. Subsequently, the evaporated HBC molecules are ionized by an EGUN and transported into the iontr chamber via the ion gate and QMF. In this chamber, another oven (neutral molecules source, ∼300 K) is located under the trap to make the vapour phase molecules (anthracene power, J&K, with a purity better than 99 per cent) effuse toward the centre of the ion trap, where the HBC/anthracene cluster cations are formed by the collision reaction between cations and neutral anthracene molecules. After a short time delay (typically ∼0.2 s) with the ion gate closed, the stored waveform inverse Fourier transform excitation (SWIFT) pulse is applied to isolate species within a given mass/charge (m/z) range (Doroshenko & Cotter 1996). Helium gas is introduced continuously into the trap to thermalize the ion cloud through collisions via a leak valve (Agilent). The working pressures in the ionso, iontr and TOF chambers are $\sim 5.0 \times 10^{-8}$, $\sim 6.0 \times 10^{-7}$ and $\sim 7.0 \times 10^{-9}$ mbar, respectively. Moreover, cluster cations are presumably formed by collision stabilization of helium atoms under our experimental operating conditions. The third harmonic laser of Nd:YAG (INDI, Spectra-Physics), 355 nm, ∼6 ns, operated at 10 Hz, 1.5 mJ (after the beam out the vacuum chamber, ∼3 mm in diameter, $\sim 2.5 \times 10^5$ W in peak power), is used to irradiate the trapped species.

The typical frequency of 0.2 Hz is used for our set-up (i.e. one full measuring cycle lasted 5 s), which benefits the accumulation of newly formed ion clusters. In our experiment, a beam shutter (Uniblitz, XRS−4) is used to act as a physical shield inside in the iontr chamber and determines the interaction time of the light and trapped ion clusters. The shutter can only be externally triggered to guarantee that the ion cloud is irradiated for a specified amount of time during each measurement cycle. We use a high-precision delay generator (SRS DG535) to control the full timing sequence to make sure that each cycle begins with an empty ion trap. The ion gate opens (0–4.0 s) at the leading edge of the master trigger, allowed the ion trap to fill for a certain amount of ions. In this period, the trapped ion collision reaction occurs between cations and anthracene molecules to form new cluster cations. Once the clusters are formed, the SWIFT technique is applied to distinguish a specific range of m/z species (4.0–4.2 s). Afterwards (i.e. ∼0.2 s), the beam shutter opens, allowing the ion cloud to be irradiated (4.4–4.9 s). At the end of irradiation, a negative square pulse is applied to the end cap of the ion trap to accelerate the ions out of the trap and transfer them into the field-free TOF region, where the mass fragments can be measured. A LABVIEW program automates the full data acquisition process. The resulting mass spectra are shown in Figs 1–4.

3 EXPERIMENTAL RESULTS AND DISCUSSION

Fig. 1 shows a typical mass spectrum of HBC/anthracene cluster cations, without either SWIFT isolation or laser irradiation. A series of peaks of HBC/anthracene cluster cations are observed, corresponding to different m/z species. Apart from the main HBC mass peak ($C_{42}H_{18}^+$, $m/z = 522$), some mainly residual HBC fragments are also measured, such as $C_{42}H_{14/15/16/17}^+$, $m/z = 518$, 519, 520, 521, namely as dehydrogenated HBC (DHBC), generated from the electron impact ionization (Zhen et al. 2014), and we only consider these fragments in the reaction pathway. In detail, the HBC/anthracene cluster cations are labelled in a zoom-in mass spectrum in Fig. 1, showing the new formed dehydrogenated HBC/anthracene cluster cations; that is, partially H-stripped ion species with the most abundant species, $C_{14}H_{10}DHBC^+$ (e.g. $C_{14}H_{10}C_{42}H_{17}^+$, $m/z = 699$), $(C_{14}H_{10})_2DHBC^+$ [e.g. $(C_{14}H_{10})_2C_{42}H_{16}^+$, $m/z = 876$] and $(C_{14}H_{10})_3DHBC^+$ [e.g. $(C_{14}H_{10})_3C_{42}H_{15}^+$, $m/z = 1053$]. In addition, we also observed one 'extra' peak ($m/z = 791$), although no assignments can be provided. We expect this peak might be formed as a side-product due to contaminations in the ion trap chamber.

The intensity ratio of cluster species is $HBC^+ : C_{14}H_{10}DHBC^+ : (C_{14}H_{10})_2DHBC^+ : (C_{14}H_{10})_3DHBC^+ = 100 : 4 : 0.6 : 0.1$. This exponential decay of the intensity ratio demonstrates that the collision formation reaction between DHBC and neutral anthracene molecules occurs step by step (Zhen et al. 2018; Zhang et al. 2019). According to our previous works (Zhen

Downloaded from https://academic.oup.com/mnras/article-abstract/486/3/3259/5480882 by University of Science and Technology of China user on 05 May 2019

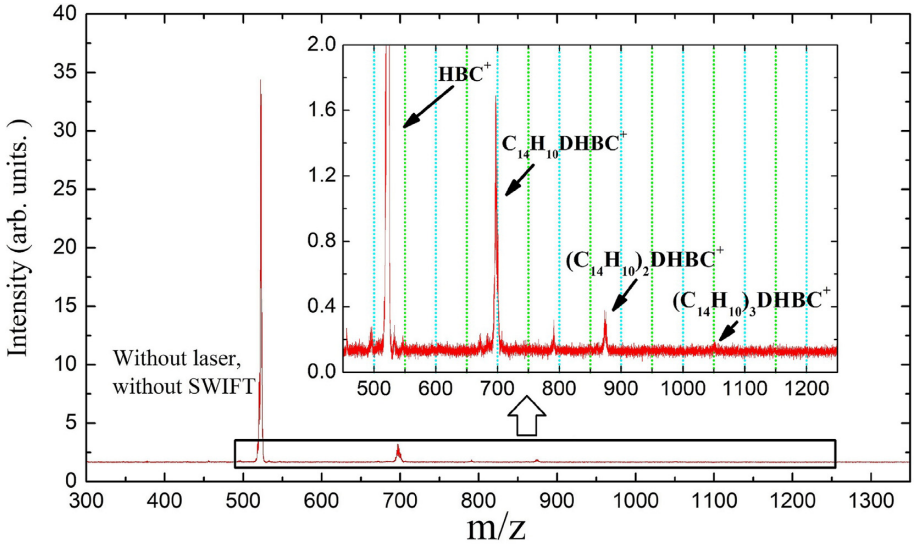

Figure 1. Mass spectrum of HBC/anthracene cluster cations trapped in the QIT before SWIFT isolation and without laser irradiation. The inset is a zoom-in mass spectrum, revealing the presence of newly formed clusters: $C_{14}H_{10}DHBC^+$, $(C_{14}H_{10})_2DHBC^+$ and $(C_{14}H_{10})_3DHBC^+$.

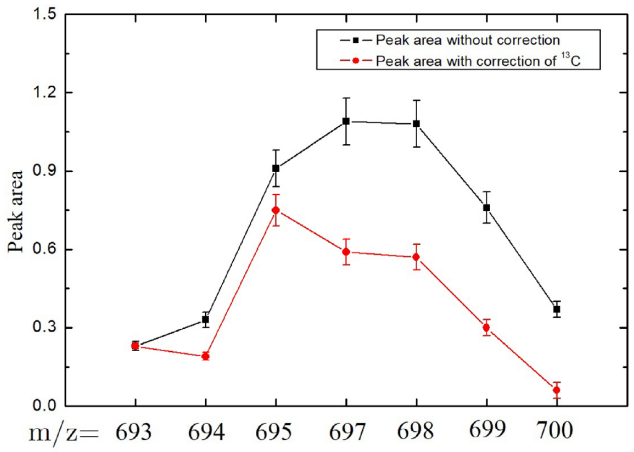

Figure 2. Peak area of $C_{14}H_{10}DHBC^+$ (without laser irradiation), with and without ^{13}C correction.

et al. 2014, 2018), we compare the peak areas of $(C_{14}H_{10})HBC$ cluster cations with and without isotope (^{13}C) correction, as shown in Fig. 2. It is clear that the $m/z = 700$ peak in Fig. 1 is mainly the covalently bonded $(C_{14}H_{10})C_{42}H_{17}^+$ cluster (i.e. $^{13}C^{12}C_{55}H_{27}^+$, $m/z = 700$), rather than the non-covalently bonded $(C_{14}H_{10})C_{42}H_{18}^+$ ($^{12}C_{56}H_{28}^+$, $m/z = 700$).

Based on the observations, we propose the following formation reactions from $C_{14}H_{10}DHBC$ to $(C_{14}H_{10})_2DHBC$, and then to $(C_{14}H_{10})_3DHBC$ cluster cations. For the group of $C_{14}H_{10}DHBC^+$ with different HBC dehydrogenated levels, we propose

$$C_{14}H_{10} + C_{42}H_{17}^+ \rightarrow C_{14}H_{10}C_{42}H_{17}^+, \quad (1)$$

$$C_{14}H_{10} + C_{42}H_{16}^+ \rightarrow C_{14}H_{10}C_{42}H_{16}^+, \quad (2)$$

$$C_{14}H_{10} + C_{42}H_{15}^+ \rightarrow C_{14}H_{10}C_{42}H_{15}^+, \quad (3)$$

$$C_{14}H_{10} + C_{42}H_{14}^+ \rightarrow C_{14}H_{10}C_{42}H_{14}^+, \quad (4)$$

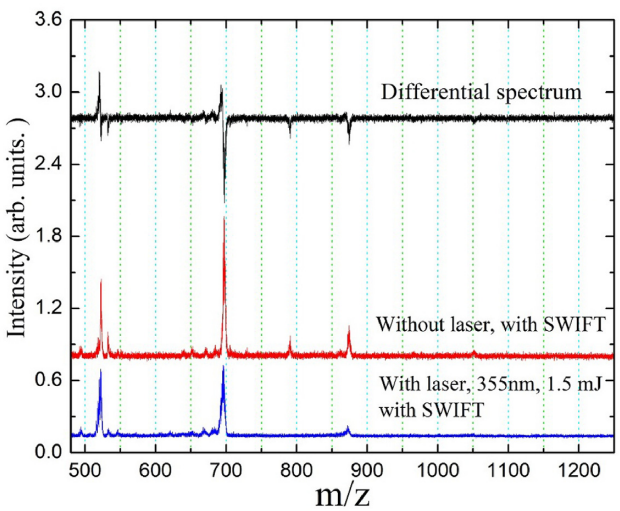

Figure 3. Mass spectrum of HBC/anthracene cluster cations: with SWIFT isolation, but without (red) and with (blue) 1.5 mJ of laser irradiation (355 nm), and the differential spectrum (black).

for the group of $(C_{14}H_{10})_2DHBC^+$ accordingly we propose

$$C_{14}H_{10} + C_{14}H_{10}C_{42}H_{16}^+ \rightarrow (C_{14}H_{10})_2C_{42}H_{16}^+, \quad (5)$$

$$C_{14}H_{10} + C_{14}H_{10}C_{42}H_{15}^+ \rightarrow (C_{14}H_{10})_2C_{42}H_{15}^+, \quad (6)$$

$$C_{14}H_{10} + C_{14}H_{10}C_{42}H_{14}^+ \rightarrow (C_{14}H_{10})_2C_{42}H_{14}^+, \quad (7)$$

and, finally, for the group of $(C_{14}H_{10})_3DHBC^+$

$$C_{14}H_{10} + (C_{14}H_{10})_2C_{42}H_{15}^+ \rightarrow (C_{14}H_{10})_3C_{42}H_{15}^+, \quad (8)$$

$$C_{14}H_{10} + (C_{14}H_{10})_2C_{42}H_{14}^+ \rightarrow (C_{14}H_{10})_3C_{42}H_{14}^+. \quad (9)$$

Fig. 3 shows the mass spectrum of trapped HBC/anthracene cluster cations upon 355 nm irradiation with 1.5 mJ of laser energy (the entire irradiation time is 0.5 s, typically with ~5 pulses),

Downloaded from https://academic.oup.com/mnras/article-abstract/486/3/3259/5480882 by University of Science and Technology of China user on 05 May 2019

with SWIFT isolation. As we can see in Fig. 3 (upper black line, differential spectrum), the intensity of lower-mass peaks is increased upon laser irradiation while the higher-mass peaks are decreased for each group of HBC/anthracene cluster cations. To understand the photo-fragmentation behaviour of the HBC/anthracene cluster cations in further detail, we illustrate the mass spectrum in Fig. 4 (zoom-in and zoom-out of Fig. 3 in detail).

From Fig. 4(a) (upper black line, differential spectrum), for the group of HBC cations, the intensity of newly formed species (lower-mass peaks, 'profit' ≈ 0.7) is more than the dissociation species (higher-mass peaks, 'loss' ≈ 0.1). However, for the group of $C_{14}H_{10}$DHBC cluster cations (see Fig. 4b, upper black line, differential spectrum), the intensity of newly formed species (lower-mass peaks, 'profit' ≈ 0.8) is less than the dissociation species (higher-mass peaks, 'loss' ≈ 1.7) with laser treatment. This phenomenon indicates that, with laser irradiation, the $C_{14}H_{10}$DHBC cluster cations not only have a dehydrogenation channel but also have a mono-anthracene dissociation channel. For the intensity of HBC^+ and $(C_{14}H_{10})DHBC^+$, the 'loss' and 'profit' peaks in the differential spectra are nearly balanced, when we do not consider other peaks. The 'extra' number of HBC species are generated from the dissociation of $C_{14}H_{10}$DHBC by the loss of its mono-anthracene group. The $C_{14}H_{10}$DHBC cations can either convert to more aromatic species by the dehydrogenation process or shrink them back to small size molecules. by breaking the C–C bond between anthracene and HBC. Based on previous work by Zhen et al. (2018) and Zhang et al. (2019), we consider that to the dehydrogenation channel of HBC/anthracene cluster cations, where the H-atom is lost from anthracene (one carbon in sp^3 hybrid orbital with a C–H bond).

In Figs 4(c) and (d) (upper black line, differential spectrum), for $(C_{14}H_{10})_2$DHBC and $(C_{14}H_{10})_3$DHBC cations, we cannot observe any newly formed species, that might only have the mono-anthracene dissociation channel.

On the basis of the above discussion, we propose the following photo-dissociation channels upon laser irradiation for the three groups of $C_{14}H_{10}$DHBC, $(C_{14}H_{10})_2$DHBC and $(C_{14}H_{10})_3$DHBC cluster cations: for the group of $C_{14}H_{10}DHBC^+$

$$C_{14}H_{10}DHBC^+ + h\nu \rightarrow C_{14}H_9DHBC^+ + H, \quad (10)$$

$$C_{14}H_{10}DHBC^+ + h\nu \rightarrow DHBC^+ + C_{14}H_{10}; \quad (11)$$

for the groups of $(C_{14}H_{10})_2DHBC^+$ and $(C_{14}H_{10})_3DHBC^+$

$$(C_{14}H_{10})_2DHBC^+ + h\nu \rightarrow C_{14}H_{10}DHBC^+ + C_{14}H_{10}, \quad (12)$$

$$(C_{14}H_{10})_3DHBC^+ + h\nu \rightarrow (C_{14}H_{10})_2DHBC^+ + C_{14}H_{10}. \quad (13)$$

4 RESULTS OF THEORETICAL CALCULATIONS AND DISCUSSION

From the discussion of the mass spectrum, we have shown that a series of cationic clusters are generated in our experiment. In this section, we employ quantum chemistry calculations to link the experimental observations with their structures and possible reaction pathways. The theoretical calculations are carried out with the hybrid density functional B3LYP (Becke 1992; Lee, Yang & Parr 1988) as implemented in the Gaussian 16 program (Frisch et al. 2016). The basis set of 6-311+ + G(2d,p) is used for all calculations. To account for the intermolecular interaction, the dispersion-correction (D3; Grimme, Ehrlich & Goerigk 2011) is also considered for each system.

From the theoretical calculations, and as in Zhen et al. (2018), $C_{14}H_{10}DHBC^+$ is a cationic cluster of mono-anthracene and HBC, connected by one C–C single bond. Here, the HBC is a dehydrogenated cation with a different dehydrogenated level (i.e. $C_{42}H_{14/15/16/17}{}^+$). Accordingly, the cationic clusters are: $[C_{14}H_{10}{-}C_{42}H_{14}]^+$ ($m/z = 696$); $[C_{14}H_{10}{-}C_{42}H_{15}]^+$ ($m/z = 697$); $[C_{14}H_{10}{-}C_{42}H_{16}]^+$ ($m/z = 698$); $[C_{14}H_{10}{-}C_{42}H_{17}]^+$ ($m/z = 699$). For the C–C single bond in the $C_{14}H_{10}DHBC^+$ cluster, one carbon from HBC is in sp^2 hybridization, and the other carbon from anthracene is in sp^3 hybridization with an additional C–H bond. The formation reaction pathways of the $C_{14}H_{10}$DHBC group cluster cations have been shown in equations (1)–(4).

As one typical example, in the following, we discuss the formation pathway of $[C_{14}H_{10}{-}C_{42}H_{17}]^+$, which is a cationic cluster consisting of a neutral anthracene and $C_{42}H_{17}{}^+$. In Fig. 5(a), we present the possible reaction pathways of equation (1) and the optimized structures of $[C_{14}H_{10}{-}C_{42}H_{17}]^+$, from the single $C_{42}H_{17}{}^+$ (positions A and B) and $C_{14}H_{10}$ (positions a, b and c) to the cationic cluster of $[C_{14}H_{10}C_{42}H_{17}]^+$ (positions Aa, Ab, Ac, Ba, Bb and Bc). As a result, there might be six different possible isomer structures for the cationic cluster. Clearly, all the reactions are exothermic in the range from –2.7 to –3.6 eV, and the formation pathway with the lowest energy is $C_{42}H_{17}{}^+$ (B) + $C_{14}H_{10}$ (b) → $[C_{14}H_{10}{-}C_{42}H_{17}]^+$ (Bb).

For the $(C_{14}H_{10})_2$DHBC group, as shown in Fig. 5(b), similarly to $C_{14}H_{10}DHBC^+$, the structure consists of two mono-anthracene molecules and one DHBC, connected by two C–C single bonds: $(C_{14}H_{10})_2C_{42}H_{14}{}^+$, $m/z = 874$; $(C_{14}H_{10})_2C_{42}H_{15}{}^+$, $m/z = 875$; $(C_{14}H_{10})_2C_{42}H_{16}{}^+$, $m/z = 876$. The DHBC fragment cations are $C_{42}H_{14/15/16}{}^+$, which at least have two dehydrogenated sites available. Equations (5)–(7) show the formation reaction pathway for $(C_{14}H_{10})_2$DHBC cations. For the $(C_{14}H_{10})_3$DHBC group cluster cations, as shown in Fig. 5(c), similarly to $C_{14}H_{10}DHBC^+$ and $(C_{14}H_{10})_2DHBC^+$, the structure consists of three mono-anthracene molecules and one DHBC, connected by three C–C single bonds: $(C_{14}H_{10})_3C_{42}H_{15}{}^+$, $m/z = 1052$ and $(C_{14}H_{10})_3C_{42}H_{16}{}^+$, $m/z = 1053$. The HBC fragment cations are ($C_{42}H_{14/15}{}^+$), which as least have three dehydrogenated sites available. Equations (8) and (9) show the formation reaction pathway for $(C_{14}H_{10})_3$DHBC cations.

Because of the existence of too many isomer structures and reaction pathways, we only give one possible structure with one possible reaction pathway (from B–B to B–Bb to Bb–Bb, and from B–B–B to B–B–Bb to B–Bb–Bb to Bb–Bb–Bb), as shown in Figs 5(b) and (c), which are based on the first step of the lowest energy reaction pathway (−3.6 eV): $C_{42}H_{17}{}^+$ (B) + $C_{14}H_{10}$ (b) → $[C_{14}H_{10}{-}C_{42}H_{17}]^+$ (Bb). In our previous studies, we have shown that the dissociation energy of H-loss is generally 2.0 eV for aliphatic carbon (sp^3) within PAH clusters (Zhen et al. 2018; Zhang et al. 2019), which is in line with the calculated covalent bond energy of these PAH cluster cations.

For PAH molecules, it is commonly accepted that excitation to an excited electronic state of a PAH molecule is followed by internal conversion (IC) to a highly excited vibrational state of the ground electronic state. Intramolecular vibrational redistribution (IVR) then quickly equilibrates the excess energy among all available vibrational states (IC and IVR occur on a time-scale of picoseconds). In covalently bonded PAH cluster cations (e.g. DHBC/anthracene cluster cations), we suppose that the time-scale of IC–IVR is similar to that of PAH molecules. In our experimental conditions, the laser irradiation occurs on a nanosecond time-scale

Downloaded from https://academic.oup.com/mnras/article-abstract/486/3/3259/5480882 by University of Science and Technology of China user on 05 May 2019

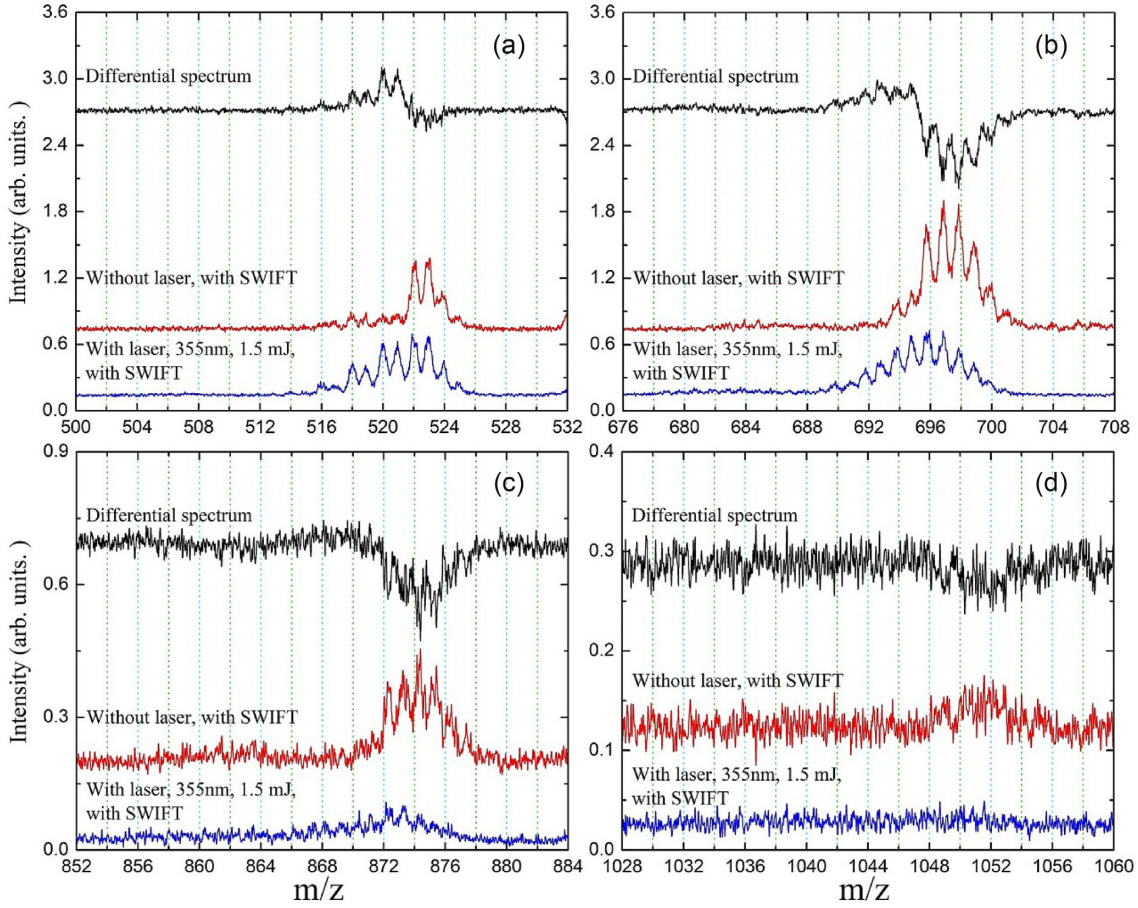

Figure 4. Mass spectrum of HBC/anthracene cluster cations, with SWIFT isolation, but without (red) and with (blue) 1.5 mJ of laser irradiation, and the differential spectrum (black): (a) in the range of m/z = 500–532 for HBC^+; (b) in the range of m/z = 676–708 for $C_{14}H_{10}DHBC^+$; (c) in the range of m/z = 852–884 for $(C_{14}H_{10})_2DHBC^+$; (d) in the range of m/z = 1028–1060 for $(C_{14}H_{10})_3DHBC^+$.

(∼6 ns). This means that all the absorbed photon energy will be converted into vibrational energy in the ground state, so we expect that the dissociation process should take place in the electronic ground state (Tielens 2008). As shown in Figs 5(b) and (c), the covalent bond energy decreases with the size increase. For the $C_{14}H_{10}DHBC$ cation, dehydrogenation (H-loss) is dominant. For the first dehydrogenation step in HBC/anthracene cluster cations, the C–H located in anthracene (carbon is in sp^3 hybrid orbital) is found to be the most favourable, and the dehydrogenation process of HBC/anthracene cluster cations is similar to that of pyrene dimer cations (Zhen et al. 2018). Following dissociation initiated by the laser irradiation, it is suspected that these covalently bonded clusters evolve towards either more aromatic species or cluster dissociation. Theoretical studies regarding the possible transition states and dynamical processes will be carried out in a subsequent paper (Zhang & Zhen, in preparation). In addition, further experiments will be needed to address the evolution of collision reactions of large neutral PAHs with PAH cations.

5 ASTRONOMICAL IMPLICATIONS

The possible formation, stability and chemical role of complexes and (PAH) clusters in space is a very interesting topic, especially with regards to large molecular clusters (>100 atoms). It has been suggested that the presence of PAH clusters can help to explain certain characteristics of the astronomical observations of the unidentified IR emission spectra (Tielens 2013). Model studies generally assume that these clusters are bonded by weak van der Waals forces (Potapov 2017). However, as pointed out, these bonds are very weak (Rhee et al. 2007), and such clusters might thus not survive a long time in the ISM (Rapacioli et al. 2006). Besides, recent experiments have shown us that the covalently bonded clusters of small PAHs can survive for a long time (even under conditions in which H-atoms are stripped off; Zhen et al. 2018; Zhang et al. 2019), even though the formation process of such clusters is not entirely clear currently and hence it is still difficult to assess their formation in the ISM. This work provides further insight into the evolution process of large covalently bonded PAH clusters (condensation). The evolution mechanism of DHBC/anthracene clusters obtained here can be generalized, which can give us a reasonable explanation for the photo-evolution of large molecular clusters and astronomically relevant and large PAHs (e.g. from $C_{14}H_{10}HBC$ to 56 C-atoms PAHs) in space (Andrews et al. 2015; Croiset et al. 2016).

Under laser irradiation, the large covalently bonded clusters will either convert to their stable forms (i.e. form more aromatic species via dehydrogenation processes) or shrink back to smaller PAH clusters or monomer species. Excitation of PAHs or PAH clusters in the ISM is mainly generated by single photon absorption. As discussed earlier, in our experimental conditions all the absorbed

Downloaded from https://academic.oup.com/mnras/article-abstract/486/3/3259/5480882 by University of Science and Technology of China user on 05 May 2019

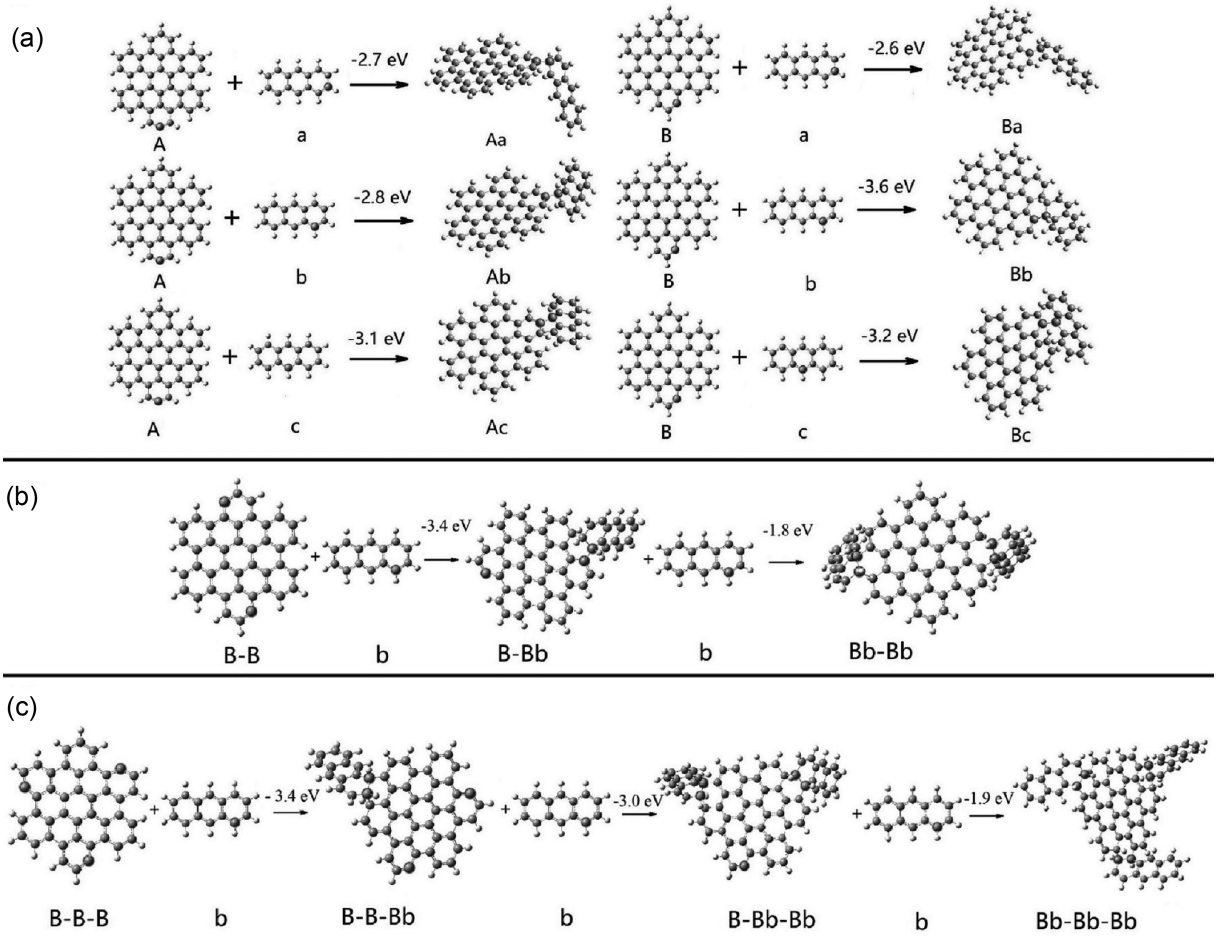

Figure 5. The upper panel (a) is the formation reaction pathway for $C_{14}H_{10}DHBC^+$ (e.g. $C_{14}H_{10}C_{42}H_{17}^+$) using equation (1). The middle panel (b) shows examples of fthe ormation reaction pathway for $(C_{14}H_{10})_2DHBC^+$ [e.g. $(C_{14}H_{10})_2C_{42}H_{16}^+$] using equations (2) and (5). The lower panel (c) is for $(C_{14}H_{10})_3DHBC^+$ [e.g. $(C_{14}H_{10})_3C_{42}H_{15}^+$] using equations (3), (6) and (8).

photon energy is converted into vibrational energy in the ground state, so the dissociation process should take place in the electronic ground state (Tielens 2008). Hence, using our experimental results, for the photoprocessing of PAHs and PAH clusters in space, as in the H I region ($5.0 < E \leqq 13.6$ eV), it is suggested that the energy of a single UV photon is capable of achieving the photodissociation process of large PAH clusters. In the ISM, the size evolution is accompanied by an evolution in the aliphatic-to-aromatic ratio (Pilleri et al. 2015; Zhen et al. 2018; Zhang et al. 2019). The present experimental and theoretical studies address these links. However, irrespective of whether dehydrogenation or shrink back are involved, the direction of the photo-evolution of molecular clusters is always towards more aromatic species (Violi & Izvekov 2007; Wang 2011; Candian, Zhen & Tielens 2018).

In addition, the structure of a pure carbon or hydrocarbon system can be more complicated in carbonaceous dust grains, as different hybridized carbon (sp, sp^2 and sp^3) and mixed hybridization states can occur in different ratios in one grain (Heidenreich, Hess & Ban 1968; Kroto et al. 1985; Jäger et al. 2011). We stress that given the different initial isomeric structures, from $C_{14}H_{10}DHBC^+$ to $(C_{14}H_{10})_2DHBC^+$ to $(C_{14}H_{10})_3DHBC^+$, in the range from 83 to 129 atoms or ∼2 nm in size, HBC/anthracene cluster is a good example of carbonaceous grains in space.

6 CONCLUSIONS

We have presented the first experiment on the formation and photo-chemistry process of large covalently bonded PAH clusters (e.g. a family group of HBC/anthracene clusters, ∼100 atoms) in the gas phase. The formation process of the HBC/anthracene cluster cation provides a possible explanation for the evolution of large molecular clusters in space. By studying the quantum chemical calculations, we demonstrate that the structure of these HBC/anthracene clusters is diverse. Subsequent photoprocessing can further convert those clusters to larger PAHs or shrink them back to small monomer PAHs. Finally, HBC/anthracene clusters, as an example of carbonaceous dust grains, provide a basic understanding of the grain evolution processes in the gas phase.

ACKNOWLEDGEMENTS

This work is supported by the Fundamental Research Funds for the Central Universities and by the National Science Foundation of China (NSFC; Grant Nos 11421303 and 11590782).

Downloaded from https://academic.oup.com/mnras/article-abstract/486/3/3259/5480882 by University of Science and Technology of China user on 05 May 2019

REFERENCES

Allamandola L. J., Tielens A. G. G. M., Barker J. R., 1989, ApJS, 71, 733
Andrews H., Boersma C., Werner M. W., Livingston J., Allamandola L. J., Tielens A. G. G. M., 2015, ApJ, 807, 99
Becker L., Bada J. L., Winans R. E., Bunch T. E., 1994, Nature, 372, 507
Becke A. D., 1992, J. Chem. Phys., 96, 2155
Berné O. et al., 2007, A&A, 469, 575
Candian A., Zhen J., Tielens A. G. G. M., 2018, Phys. Today, 71, 38
Castellanos P., Candian A., Zhen J., Linnartz H., Tielens A. G. G. M., 2018, A&A, 616, A166
Chen H. X., Dobbins R., 2000, Combustion Science and Technology, 159, 109
Croiset B. A., Candian A., Berné O., Tielens A. G. G. M., 2016, A&A, 590, A26
Doroshenko M. V., Cotter R. J., 1996, Rapid Communications in Mass Spectrometry, 10, 65
Ekern S. P., Marshall A. G., Szczepanski J., Vala M., 1998, J. Phys. Chem. A, 102, 3498
Elvati P., Violi A., 2013, Proc. Combust. Inst., 34, 1837
Frisch M. J. et al., 2016, Gaussian 16 revision e. 01. Gaussian Inc., Wallingford, CT
Grimme S., Ehrlich S., Goerigk L., 2011, Journal of Computational Chemistry, 32, 1456
Heidenreich R., Hess W., Ban L., 1968, Journal of Applied Crystallography, 1, 1
Henning T., Salama F., 1998, Science, 282, 2204
Jäger C., Huisken F., Mutschke H., Llamas Jansa I., Henning T., 2009, ApJ, 696, 706
Jäger C., Mutschke H., Henning T., Huisken F., 2011, in Joblin C., Tielens A. G. G. M., eds, EAS Pub. Ser. Vol. 46, PAHs and the Universe. EDP Sciences, Les Ulis, p. 293
Kroto H., Heath J., O'Brien S., Curl R., Smalley R., 1985, Nature, 318, 162
Le Page V., Snow T. P., Bierbaum V. M., 2001, ApJS, 132, 233
Lee C., Yang W., Parr R. G., 1988, Phys. Rev. B, 37, 785
Pilleri P., Joblin C., Boulanger F., Onaka T., 2015, A&A, 577, A16
Potapov A., 2017, Molecular Astrophysics, 6, 16
Puget J. L, Leger A., 1989, ARA&A, 27, 161
Rapacioli M., Joblin C., Boissel P., 2005, A&A, 429, 193
Rapacioli M., Calvo F., Joblin C., Parneix P., Toublanc D., Spiegelman F., 2006, A&A, 460, 519
Rhee Y. M., Lee T. J., Gudipati M. S., Allamandola L. J., Head-Gordon M., 2007, Proceedings of the National Academy of Science, 104, 5274
Richter H., Howard J. B., 2000, Progress in Energy and Combustion Science, 26, 565
Richter H., Granata S., Green W. H., Howard J. B., 2004, Proc. Combust. Inst., 30, 1397
Sellgren K., 1984, ApJ, 277, 623
Tielens A. G. G. M., 2005, The Physics and Chemistry of the Interstellar Medium, 1st edn. Cambridge Univ. Press, Cambridge
Tielens A. G. G. M., 2008, ARA&A, 46, 289
Tielens A. G. G .M., 2013, Rev. Mod. Phys., 85, 1021
van Diedenhoven B., Peeters E., Van Kerckhoven C., Hony S., Hudgins D. M., Allamandola L. J., Tielens A. G. G. M., 2004, ApJ, 611, 928
Violi A., Izvekov S., 2007, Proc. Combust. Inst., 31, 529
Wang H., 2011, Proc. Combust. Inst., 33, 41
West B., Castillo S. R., Sit A., Mohamad S., Lowe B., Joblin C., Bodi A., Mayer P. M., 2018, Physical Chemistry Chemical Physics, 20, 7195
Zhang W., Si Y. B., Zhen J., Chen T., Linnartz H., Tielens A. G. G. M., 2019, ApJ, 872, 38
Zhen J., Paardekooper D. M., Candian A., Linnartz H. Tielens A. G. G. M., 2014, Chem. Phys. Lett., 592, 211
Zhen J., Castellanos, Bouwman J. D. M., Linnartz H., Tielens A. G. G. M., 2017, ApJ, 836, 28
Zhen J., Chen T., Tielens A. G. G. M., 2018, ApJ, 863, 128

This paper has been typeset from a TEX/LATEX file prepared by the author.

Downloaded from https://academic.oup.com/mnras/article-abstract/486/3/3259/5480882 by University of Science and Technology of China user on 05 May 2019